

DEM study on mixing behaviors of concave-shaped particles in rotating drum based on level-set method

Siqiang Wang^a, Dongfang Liang^b, Shunying Ji^{a,*}

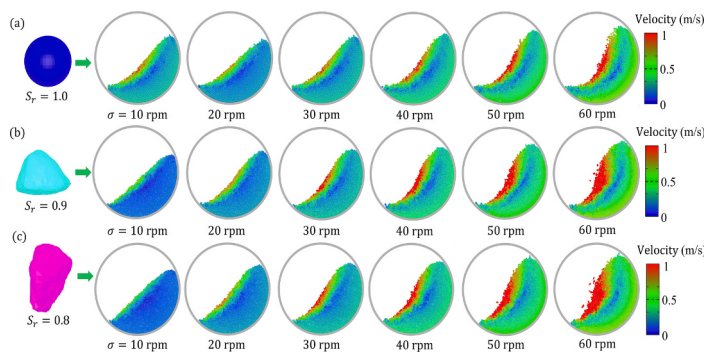
^a State Key Laboratory of Structural Analysis, Optimization and CAE Software for Industrial Equipment, Dalian University of Technology, Dalian 116024, China

^b Department of Engineering, University of Cambridge, Cambridge CB2 1PZ, UK

HIGHLIGHTS

- Concave-shaped particles are modeled by the spherical harmonic functions.
- The normal overlaps between concave particles are obtained by the level set method.
- The mixing properties of spherical and concave particles in the drum are compared.
- The mixing rate of concave particles decreases with decreasing particle sphericity.
- Concave particles have closer contact modes and larger contact forces than spheres.

GRAPHICAL ABSTRACT



ARTICLE INFO

Keywords:
Discrete element method
Level-set method
Spherical harmonic particles
Concave shape
Mixing behaviors

ABSTRACT

Granular mixing is a complex phenomenon that is commonly encountered in various engineering disciplines. A large number of past studies have mainly focused on the mixing properties of convex-shaped granular materials, while the mixing behaviors of concave-shaped granular materials have not been well studied. In this study, spherical harmonic functions are used to describe the spherical and concave shapes of individual particles. The level set function is an implicit function consisting of a set of points that can be used to determine the contact points between particles. Then, the influences of the particle shape and rotational speed on the mixing behaviors of the granular material within a horizontal drum are analyzed by the discrete element method (DEM). Results indicate that concave particles have higher coordination numbers and closer contact patterns than spherical particles, which results in greater normal collision forces, larger dynamic angle of repose and lower mixability.

1. Introduction

The rotating drum is commonly applied in industries, including segregation, blending, stirring, and cladding processes [1–3]. The discrete element method (DEM) is a pivotal tool for understanding the

mixing characteristics of particles within rotating drums, and the mechanistic analysis of granular materials at macroscopic and microscopic scales is essential for the design and optimization of industrial equipment [4–7]. The DEM research on the mixing properties of the granular material within rotating drums focuses on the effects of the

* Corresponding author.

E-mail address: jisy@dlut.edu.cn (S. Ji).

rotating velocity, shape and size of the structure as well as the filling fraction, elastic modulus, friction coefficient and basic shape of particles on the mixing degree, duration and particle temperature [8–10]. The physical mechanisms of particle mixing included particle convection, dispersion and separation, and the internal baffles in the drum tended to restrain the free surface flow of particles and enhance particle mixing [11,12]. Particle motion in the mixer included sliding, avalanche, cascade, cataract and centrifugation, and collisions between particles were the main factors affecting particle mixing and dispersion [6]. The mixer shape was used to improve the mixing efficiency of particles, and the mixing speed of particles in the 4-bladed mixer was faster than that of particles in the 2-bladed mixer [13]. Although Young's modulus significantly affected the collision time and rebound behavior between two particles, its effect on the mixing behaviors of particles was not evident [14]. However, the aforementioned researches mainly contributed to the DEM investigation of the mixing properties of the spherical granular material within rotating drums, while few studies were performed on the mixing behaviors of convex and concave-shaped granular materials.

In recent years, the flow behaviors of nonspherical particles within rotating drums have been widely studied [15]. Ellipsoidal and superquadric equations can be used to construct ellipsoids, cylinders, and cubic particles with different aspect ratios and surface sharpness by changing functional parameters [16]. Ellipsoidal particles had a larger average coordination number compared to spherical particles [17], and the mixing rate of ellipsoidal particles increased and then decreased with increasing aspect ratios [18]. The super-ellipsoid model was used for rod-like particles, and the mixing rate of particles increased with decreasing aspect ratio or increasing rotation speed [19]. However, the particle shapes constructed by ellipsoidal and superquadric equations are centrosymmetric, which narrows the practical applications of these models [20]. The soft sphere imbedded pseudo-hard-particle approach was used to study the mixing process of polyhedrons within the rotational drum, and the squares, hexagons and triangles of granular materials were more highly mixed than the pentagon, heptagon, octagon, and decagon [21,22]. Besides, particle shape and density significantly affected the uniformity of mono- and bi-disperse sphero-cylinder mixtures, and most particles were spatially oriented perpendicular to the rotational direction to achieve minimal energy dissipation [23]. It is worth noting that particles constructed by different nonspherical DEM models had different flow and mixing properties [24]. Polyhedral particles had sharper corners and stronger interlocking than smooth polyhedrons, which resulted in larger dynamic angles of repose and more inhomogeneous particle motion than smooth polyhedrons [25]. However, polyhedral and smooth polyhedral models are only suitable for DEM simulations of convex-shaped granular materials due to the limited availability of contact algorithms [26]. Therefore, the mixing behaviors of concave-shaped granular materials need to be further investigated.

In recent review studies, discrete element methods for concave granular materials have become a topical and challenging problem [27,28]. Compared to convex particles, concave particles have multiple collisions, low flowability and strong interlocking properties [29]. The discrete element methods for concave particles include combined particle models and single particle models [28]. In the combined particle model, multiple basic particles are combined with different overlaps, numbers, sizes and spatial orientations to describe arbitrary morphological particles [30]. The morphology of these basic particles is convex, including spheres, ellipsoids, cylinders, polyhedrons, super-ellipsoids, and sphero-cylinders [31–33]. The contact detection between concave particles can be simplified to the contact detection between multiple convex particles, which avoids the complicated contact detection between concave particles [34]. However, the combined particle model introduced shape errors at the single particle level, and the computational efficiency decreased as the number of basic particles increased [35]. Another method of representing concave particles is single particle models, including the heart-shaped model [36], spherical harmonic

functions [37], non-uniform rational basis splines (NURBS) [38,39], random field theory [40], Fourier series [41], level set functions [42], signed distance field [43] and energy conservation theory [44,45]. Among these methods, spherical harmonic particles are a crucial class of concave-shaped granular materials, including most industrial particles, particles extracted from the earth, and certain biological particles in living organisms [46]. The spherical harmonic functions prove to be effective in constructing irregular particles with uneven surfaces, and this model combined with X-ray computed tomography can be used to reconstruct the actual particle morphology [47]. Particle abrasion was modeled by removing the higher terms of the spherical harmonic expansion, and then particles with sharp vertices and edges became particles with smooth surfaces [48]. Spherical harmonic particles are used to construct concave fillers in composite materials and combined with Monte Carlo and GPU parallel methods to calculate the volume fraction of interfacial transition zones [49–51]. Compared to spherical particles, spherical harmonic particles had higher strength and dilatancy in the triaxial compression [52]. Meanwhile, spherical harmonic granular materials had slower velocities and more pronounced fluctuations in silos than spherical particles [53]. Although the spherical harmonic function can be used to efficiently construct concave-shaped particles, accurate calculations of contact forces are still commonly based on multi-sphere models [54], and the mixing properties of spherical harmonic particles have rarely been discussed.

In this study, the spherical harmonic function is employed to represent spherical and concave-shaped particles with different sphericity, and a level set method is applied for calculating the normal overlap and direction between spherical harmonic particles. Subsequently, the discrete element method is performed for the investigation of the mixing motion of the spherical harmonic particles within a horizontally rotating drum. Besides, the effects of the particle sphericity, shape parameter, and rotating speed on the mixing processes and velocity distribution of spherical harmonic particles are analyzed. Moreover, the Lacey mixing index, dynamic angle of repose, average coordination number, total kinetic energy and normal contact force of the particles are discussed to gain insight into the mixing characteristics of concave-shaped particles.

2. Method for modeling concave-shaped particles

2.1. Representation of spherical harmonic function

The spherical harmonic function represents a mathematical model that defines convex and concave morphologies in a spherical coordinate system. It is widely used in different fields and represents different types of real particles, such as sand [55], rock [56], crushed gravel [46], and lunar soil [46]. This mathematical function can be expressed as [57]:

$$r(\theta, \varphi) = \sum_{n=0}^N \sum_{m=-n}^n A_{nm} Y_n^m(\theta, \varphi) \quad (1)$$

where r denotes the radial distance of the surface point, illustrated in Fig. 1(a). θ denotes an angle between the length r and the z -direction. φ denotes an angle between the length r and the x -direction. A_{nm} denotes the spherical harmonic coefficient. N denotes the shape parameter. $Y_n^m(\theta, \varphi)$ is given as [58]:

$$Y_n^m(\theta, \varphi) = \sqrt{\frac{(2n+1)(n-m)!}{4\pi(n+m)!}} P_n^m \cos(\theta) e^{im\varphi} \quad (2)$$

where m and n are the orders of P_n^m . P_n^m is the associated Legendre polynomial, expressed as:

$$P_n^m(x) = (-1)^m \frac{1}{2^n n!} (1-x^2)^{\frac{m}{2}} \frac{d^{m+n}}{dx^{m+n}} (x^2 - 1)^n, (m \geq 0) \quad (3)$$

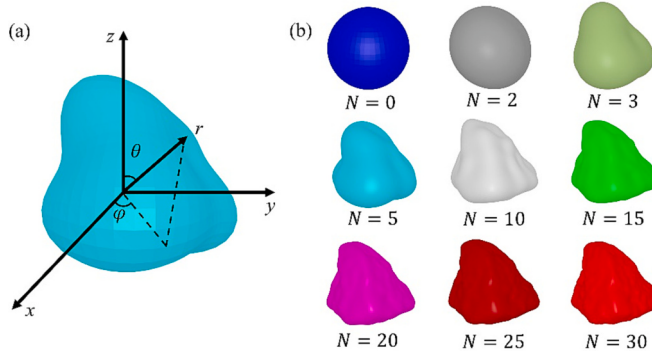


Fig. 1. (a) A three-dimensional schematic of a spherical harmonic particle. (b) Spheres and concave-shaped particles with various unevenness properties represented by changing the parameter N .

$$P_n^m(x) = (-1)^{-m} \frac{(n+m)!}{(n-m)!} P_n^{-m}(x), (m < 0) \quad (4)$$

where $n \in [0, N]$ and $m \in [-n, n]$. If $N = 0$, a sphere is obtained. The concave and convex properties of the particle surface become more significant with increasing shape parameter N , illustrated in Fig. 1(b). Although the spherical harmonic function has a great advantage in constructing particles with concave and convex morphology, it is not suitable for representing particles with internal cavities and cantilever structures. In addition, particle attrition is an essential mechanical behavior during the grinding and mixing process, which leads to changes in particle shape [48]. In future studies, the attrition characteristics of particles constructed with spherical harmonic functions will be further investigated.

2.2. Representation of level set function

In consideration of the computational complexity of contact detections between spherical harmonic particles, all spherical harmonic particles are reconstructed as level set functions [59]. This indicates that each particle is represented as a zero level set function and a spatial level set function. The level set function is actually a distance field function consisting of a series of points. The functional value D_p denotes the closest distance from discrete point P to the surface, expressed as [60]: $D_p = F(P)$. If $D_p < 0$, point P is inside the particle; If $D_p = 0$, point P is on the particle surface; If $D_p > 0$, point P is outside the particle.

A nonspherical particle with a concave surface is constructed using Eq. (1), illustrated in Fig. 2(a). To establish the corresponding zero level set function, spatial points are generated at equal distances on the bounding box for this particle. Subsequently, surface points are established by mapping all discrete points to the particle surface, illustrated in Fig. 2(b). Thus, the zero level set function actually consists of several surface points. To establish the corresponding spatial level set functions, spatial points are generated at equal distances within the bounding box

for this particle. Then, the position relationship between the discrete points and the spherical harmonic particle needs to be determined. The intersection number of rays passing through a discrete point with this particle surface is calculated using the odd–even rule approach [61]. The value (D_p) of the discrete point located outside the particle is equal to 1, while the value (D_p) of the discrete point located inside the particle is equal to -1. Secondly, each particle is meshed with a series of triangular elements, and the minimum distance (D_{\min}) from the discrete point to the surface is obtained by the point-to-triangulation distance function [62]. Therefore, the functional value of this point is expressed as: $D_p = D_p D_{\min}$. The spatial level set function is determined through the calculations of all discrete points, illustrated in Fig. 2(c).

2.3. Calculation of normal overlap and direction

Hard and soft sphere models are widely used in DEM simulations [63]. In the hard-sphere model, collisions between particles are instantaneous [64]. The overlap between particles does not need to be calculated, and the energy loss is determined by the normal and tangential restitution coefficients. In the soft-sphere model, the collision process between particles lasts for a period of time [65]. The overlap between particles needs to be calculated, and the energy loss is determined by the normal and tangential damping coefficients. In this study, the soft-sphere model is used for DEM simulations, and the level set method is used to calculate the normal direction and overlap between particles.

Two neighboring particles are denoted as i and j , and the zero level set point (P_i) of particle i is brought into the spatial level set function of particle j , illustrated in Fig. 3(a) and (b). The spatial points are equally spaced on the principal axis and satisfy as: $d_x = d_y = d_z = d_0$. Thus, the eight level set points surrounding the point P_i can be searched quickly, illustrated in Fig. 3(c). The relative coordinates of the point P_i is obtained as:

$$\begin{cases} x = (P_{ix} - P_{000,x})/d_0 \\ y = (P_{iy} - P_{000,y})/d_0 \\ z = (P_{iz} - P_{000,z})/d_0 \end{cases} \quad (5)$$

The trilinear interpolation approach is employed for calculating the functional value for point P_i , expressed as [66]:

$$\begin{aligned} D_{Pi} &= \psi(P_i) \\ &= \sum_{a=0}^1 \sum_{b=0}^1 \\ &\quad \times \sum_{c=0}^1 \psi_{abc} [(1-a)(1-x)+ax][(1-b)(1-y)+by][(1-c)(1-z)+cz] \end{aligned} \quad (6)$$

Subsequently, the functional gradient at point P_i is determined by the trilinear interpolation approach and obtained as [66]:

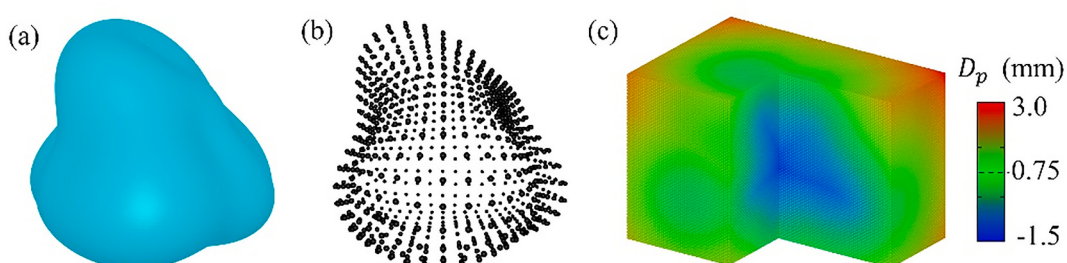


Fig. 2. A spherical harmonic particle and the associated level set functions: (a) a spherical harmonic particle; (b) the corresponding zero level set function; (c) the corresponding spatial level set function.

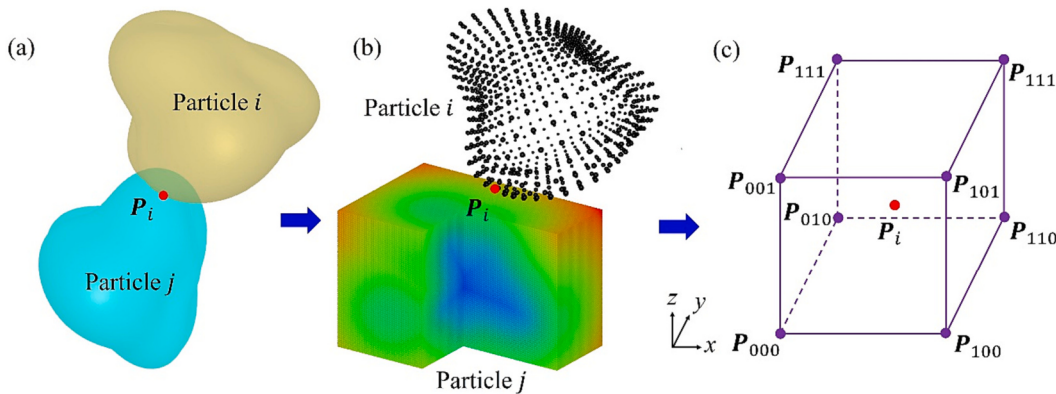


Fig. 3. (a) A schematic diagram of concave particles in contact with each other. (b) Solution of two level set functions. (c) Eight level set points surrounding point P_i .

$$\frac{\partial\psi(\mathbf{P}_i)}{\partial x} = \sum_{a=0}^1 \sum_{b=0}^1 \sum_{c=0}^1 \psi_{abc} (2a-1)[(1-b)(1-y)+by][(1-c)(1-z)+cz] \quad (7)$$

$$\frac{\partial\psi(\mathbf{P}_i)}{\partial y} = \sum_{a=0}^1 \sum_{b=0}^1 \sum_{c=0}^1 \psi_{abc} [(1-a)(1-x)+ax](2b-1)[(1-c)(1-z)+cz] \quad (8)$$

$$\frac{\partial\psi(\mathbf{P}_i)}{\partial z} = \sum_{a=0}^1 \sum_{b=0}^1 \sum_{c=0}^1 \psi_{abc} [(1-a)(1-x)+ax][(1-b)(1-y)+by](2c-1) \quad (9)$$

The particles i and j are in contact if $D_{pi} \leq 0$. The normal overlap and direction between particles are expressed as: $\delta_n = D_{pi} \cdot \mathbf{n}$ and $\mathbf{n} = \nabla\psi(\mathbf{P}_i)$, respectively.

2.4. Particle governing equations

In the DEM simulation, each particle has translational and rotational motions, expressed as:

$$m_i \frac{d\mathbf{v}_i}{dt} = \sum_{j=1}^{N_c} (\mathbf{F}_{n,ij} + \mathbf{F}_{t,ij}) + m_i \mathbf{g} \quad (10)$$

$$I_i \frac{d\boldsymbol{\omega}_i}{dt} = \sum_{j=1}^{N_c} (\mathbf{M}_{n,ij} + \mathbf{M}_{t,ij} + \mathbf{M}_{r,ij}) \quad (11)$$

where m_i and I_i denote the mass and inertia tensor of particle i , respectively. \mathbf{v}_i and $\boldsymbol{\omega}_i$ denote the translational velocity and angular velocity of particle i , respectively. $\mathbf{F}_{n,ij}$ and $\mathbf{F}_{t,ij}$ denote the normal force and tangential force, respectively. $\mathbf{M}_{n,ij}$ and $\mathbf{M}_{t,ij}$ denote the torques contributed by the forces $\mathbf{F}_{n,ij}$ and $\mathbf{F}_{t,ij}$. $\mathbf{M}_{r,ij}$ denotes the rolling friction torque. N_c denotes the total number of neighboring particles of particle i . Note that the nonlinear contact force model for spherical particles has been successfully developed. Subsequently, the contact force model for spheres was effectively extended to ellipsoids [67], super-ellipsoids [68], cylinders [69], spherocylinders [70], and arbitrarily convex particles [71]. Therefore, this contact force model is applied to spherical harmonic particles, summarized in Table 1.

3. Simulation conditions

The nonspherical granular mixing within horizontally rotating drums is widespread in industries, and the particle shapes have considerable effects on the dynamic properties and mechanical response of the granular material. The number of granular materials is 10,000, and the total mass is about 0.84 kg. All particles have an identical

Table 1
Nonlinear contact force model for spherical harmonic particles.

Forces and Torques	Symbols	Equations
Normal elastic force	$\mathbf{F}_{n,ij}^e$	$4/3E^* \sqrt{R^*} \delta_n^{3/2}$
Normal damping force	$\mathbf{F}_{n,ij}^d$	$C_n (8m^* E^* \sqrt{R^*} \delta_n)^{1/2} \bullet \mathbf{v}_{n,ij}$
Tangential elastic force	$\mathbf{F}_{t,ij}^e$	$\mu_s F_n^e \left(1 - (1 - \min(\delta_t, \delta_{t,max}) / \delta_{t,max})^{3/2} \right) \bullet \bar{\mathbf{t}}$
Tangential damping force	$\mathbf{F}_{t,ij}^d$	$C_t (6\mu_s m^* F_n^e \sqrt{1 - \min(\delta_t, \delta_{t,max}) / \delta_{t,max}})^{1/2} \bullet \mathbf{v}_{t,ij}$
Coulomb friction force	$\mathbf{F}_{t,ij}^f$	$\mu_s F_n^e \bullet \bar{\mathbf{t}}$
Torque by normal force	$\mathbf{M}_{n,ij}$	$R_{ij} \times (F_{n,ij}^e + F_{n,ij}^d)$
Torque by tangential force	$\mathbf{M}_{t,ij}$	$R_{ij} \times (F_{t,ij}^e + F_{t,ij}^d)$
Rolling friction torque	$\mathbf{M}_{r,ij}$	$\mathbf{M}_r = \mu_s R_i F_{n,ij} \hat{\omega}_{ij}$

where $E^* = E/2(1-\nu^2)$, $R^* = R_i R_j / (R_i + R_j)$, $m^* = m_i m_j / (m_i + m_j)$, $\hat{\omega}_{ij} = \omega_{ij} / |\omega_{ij}|$, $\bar{\mathbf{t}} = \delta_t / |\delta_t|$, $\delta_{t,max} = \mu_s (2-\nu) / 2(1-\nu) \cdot \delta_n$.

Note that $F_{t,ij}$ should be replaced by $F_{t,ij}^{\max}$ when $\delta_t > \delta_{t,max}$.

volume, and the diameter of the equivalent sphere is 4 mm. Sphericity was first defined by Wadell in 1933 as the ratio of the surface area of a sphere having the same volume to the actual surface area of the particles [72]. Subsequently, the sphericity is widely used for characterizing non-spherical particles constructed by the superquadric equation and spherical harmonic function [73–75]. In this study, the sphericity (S_r) is utilized for quantifying the morphological changes of the particles, expressed as [75]:

$$S_r = \frac{S_A}{S_p} = \frac{\pi^{1/3} (6V_r)^{2/3}}{S_p} \quad (12)$$

where S_p and V_r are the surface area and volume of the particle, respectively. S_A is the surface area of the volume equivalent sphere. The surface of the spherical harmonic particle is discretized into millions of triangular elements, and the sum of the triangular surface areas approximates the value S_p . Different morphological particles are constructed by changing the coefficient A_{nm} , illustrated in Fig. 4. Besides, particles with various concavities are modeled through the variation of the shape parameter N , illustrated in Fig. 5. The left illustration shows the spherical harmonic particle, and the middle illustration shows the corresponding zero level set function. The right illustration shows the corresponding spatial level set function, and the absolute value of the function is used for representing the particle morphology clearly.

The drum has a radius and length of 0.1 and 0.05 m, illustrated in

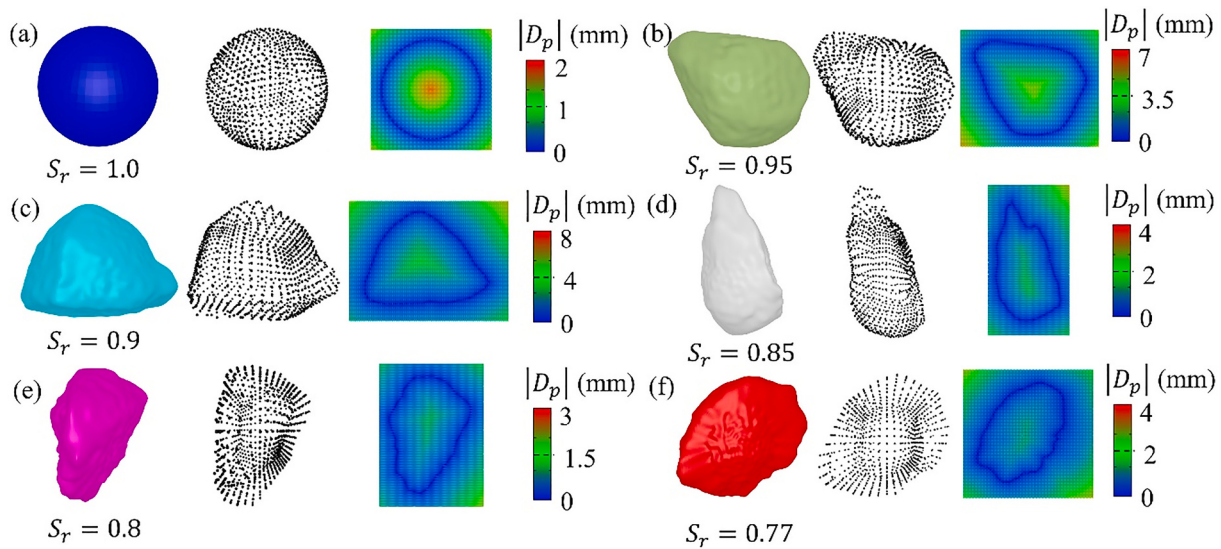


Fig. 4. Spherical harmonic particles with various sphericity and the associated level set functions: (a) $S_r = 1.0$; (b) $S_r = 0.95$; (c) $S_r = 0.9$; (d) $S_r = 0.85$; (e) $S_r = 0.8$; (f) $S_r = 0.77$.

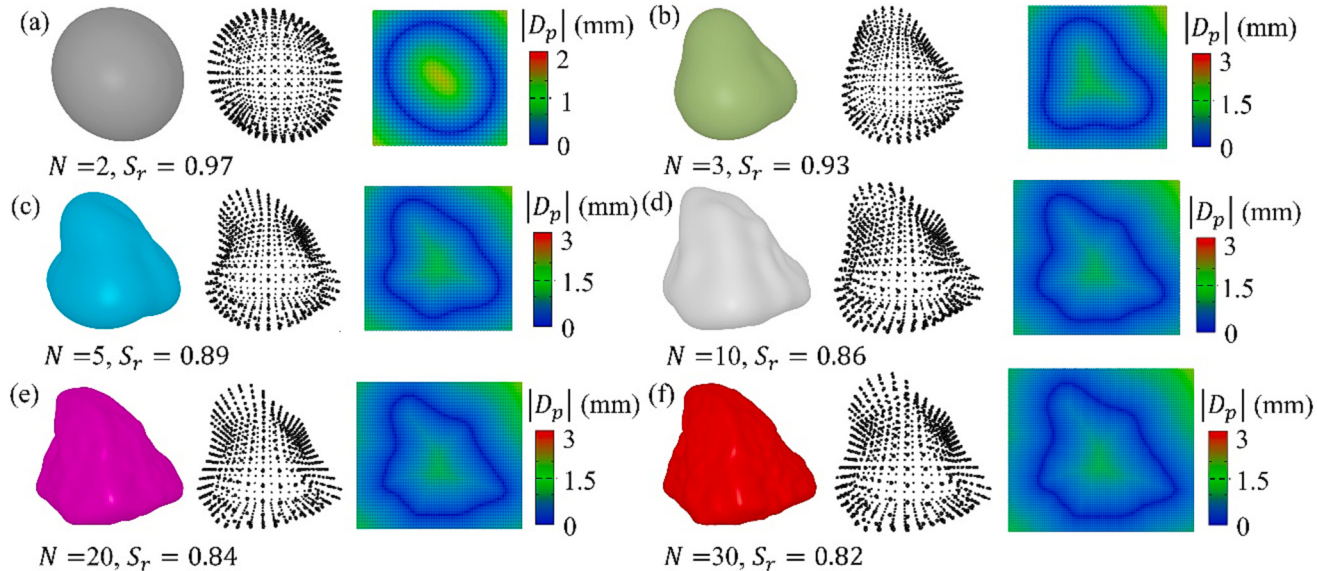


Fig. 5. Spherical harmonic particles with various shape parameters N and the associated level set functions: (a) $N = 2$; (b) $N = 3$; (c) $N = 5$; (d) $N = 10$; (e) $N = 20$; (f) $N = 30$.

Fig. 6. The rotating velocities (σ) of 10, 20, 30, 40, 50, and 60 rpm are used for spherical harmonic granular materials to reveal the cumulative effects of the drum operation. The DEM calculated parameters of the spherical harmonic granular materials are given in Table 2. At the initial moment, all spherical harmonic particles with random positions and spatial orientations are generated above the horizontal drum. The particles fall under gravity and eventually have no relative motion. If the component of the particle's central position in the x-direction is less than zero, the particle is represented in blue. Otherwise, it is represented in red.

To quantify the influence of particle shapes on the mixing behavior of granular materials, the Lacey mixing index is adopted to calculate the mixing degrees of granular materials, expressed as [76]:

$$M = \frac{S_0^2 - S^2}{S_0^2 - S_r^2} \quad (13)$$

where M denotes the Lacey mixture index. S_0^2 denotes the variance of the

granular material at complete separation, expressed as $S_0^2 = p(1-p)$. Here, p denotes the volume proportion of a specific particle category within the granular material. S_r^2 denotes the variance of the particle system when it is completely mixed, expressed as $S_r^2 = p(1-p)/N_a$. N_a denotes the average number of particles within one sample. S^2 denotes the variance of the mixture at the current moment, expressed as [11]:

$$S^2 = \frac{1}{k} \sum_{i=1}^{N_s} k_i (a_i - \bar{a})^2 \quad (14)$$

where N_s denotes the total number of samples. The rotating drum is discretized into several cubic samples, and each cube has dimensions of $3D_s \times 3D_s \times 3D_s$. D_s denotes the diameter of the equivalent sphere. k_i denotes the weight of each sample, obtained as the ratio of the particle number within sample i to the total number of particles. This means that the weight of the sample located in the upper part of the drum is zero due to the absence of particles. k denotes the number of weights added

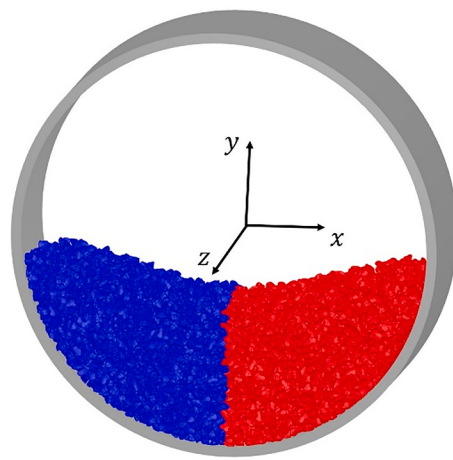


Fig. 6. A schematic diagram of a horizontally rotating drum simulated using the spherical harmonic DEM model.

Table 2
DEM parameters of spherical harmonic particles.

Definition	Value	Definition	Value
Particle density ρ , (kg/m^3)	2500	Normal damping coefficient C_n , (-)	0.3
Young's modulus E , (Pa)	1×10^7	Tangential damping coefficient C_t , (-)	0.3
Poisson's ratio ν , (-)	0.3	Sliding friction coefficient μ_s , (-)	0.3
Rolling friction coefficient μ_r , (-)	0.002		

up for all samples. a_i denotes the volume ratio of one type of particles within sample i . \bar{a} denotes the average volume ratio of one type of particles within the drum.

During the mixing processes of the granular material, the time variation of the Lacey mixing index can be fitted with the integral function, expressed as [77]:

$$M(t) = M_0 + (M_f - M_0) 2 / \sqrt{\pi} \int_0^{M_r t} e^{-(M_r t)^2} d(M_r t) \quad (15)$$

where M_0 is the unmixed Lacey mixing index and is equal to 0. M_f is the Lacey mixing index for complete mixing and is equal to 1. M_r is the mixing rate, obtained through fitting the mixing index.

4. Results and discussion

4.1. Experimental validation of the DEM model

To validate the reliability of the DEM model, prolate ellipsoidal particles are constructed using the spherical harmonic function, and the corresponding level set functions are created for this particle using the level set method, as shown in Fig. 7(a). The semi-axis lengths of the ellipsoid are 2.5, 2.5 and 5 mm, respectively. The drum has a radius and length of 0.1 and 0.02 m, and the rotating velocity (σ) of 20 rpm is used for ellipsoidal granular materials. Young's modulus, Poisson's ratio, and particle density are 1×10^8 Pa, 0.3, and $1150 \text{ kg}/\text{m}^3$, respectively. The coefficients of damping, sliding friction and rolling friction between particles are 0.3, 0.3 and 0.002, respectively. A granular material consisting of 1000 blue and red ellipsoids is generated in a drum, and all particles have random positions and spatial orientations. The particles are dropped by gravity, and the drum starts to rotate when there is no relative motion between the particles. The experimental [78] and simulation results of the mixing process of ellipsoidal granular materials

are compared, as shown in Fig. 7(b-c). The red and blue ellipsoids are gradually mixed as the number of revolutions increases, and the Lacey mixing index of the granular material is counted, as shown in Fig. 8. Although the numerical results obtained by the discrete element method have some deviation from the experimental results, the level set method is applicable for simulating the flow and mixing behaviors of spherical harmonic granular materials.

4.2. Mixing processes and flow patterns

Fig. 9 shows screenshots of the mixing processes of spherical and concave particles with various sphericity. Here, the rotating speed $\sigma = 30$ rpm. Evidently, the granular systems have entered a cascading mode, leading to the observation of an S-shaped bed surface. Near the drum, granular materials are consistently lifted, followed by experiencing collapses and flowing downwards on the bed surface. With the repeated rotation of the granular bed, the two-colored particles gradually form helical shapes and develop layered patterns. Once the rotation time exceeds six seconds, these patterns vanish, and the two colored particles become evenly dispersed within the drum. Moreover, the particle shape determines the mixing pattern of the granular material, and spherical particles exhibit better mixability than spherical harmonic particles.

Fig. 10 shows the velocity distribution of particles with various sphericity. Here, the rotational speeds $\sigma = 10, 20, 30, 40, 50, 60$ rpm. The flow field exhibits three distinct regions: a moving region near the wall, a stable region at the core of the bed, and a collapsing region on the bed surface. The stratification patterns of particle velocities become more significant with increasing rotational speed or decreasing particle sphericity. Generally, nonspherical particles close to walls are more easily lifted and consequently exhibit higher velocities compared to spheres. Thus, the surface of a spherical harmonic granular bed displays relatively greater velocities than that of a spherical granular bed. With higher rotational speeds, the regions of both the moving and collapsing layers are expanded, while the region of the stable layer is decreased. This indicates that the spherical harmonic granular materials obtain more external energy and have a higher translational velocity than the spherical granular materials at the identical rotational velocity.

4.3. Influence of particle shapes on the mixing rate

Fig. 11 shows the time variations of the mixing index of the granular material. Here, the solid line is the fitted curve of the mixing rate obtained by Eq. (15). The Lacey mixing indices of both spherical and spherical harmonic granular materials increase with time and approach 1. The Lacey mixing index of the differently shaped granular materials remains basically unchanged when the rotation time exceeds 40s. Thus, the differently shaped particles have the same end time, and the end time is 40s. Subsequently, the mixing rates of spherical and spherical harmonic granular materials with various sphericity and shape parameters are counted, illustrated in Fig. 12. The mixing rate of different morphological particles increases with increasing the rotational speed. Spheres have a faster mixing rate than spherical harmonic particles at the same rotational speed, while the mixing rates of spherical harmonic particles decrease as the sphericity decreases. Besides, the shape parameter has insignificant effects on the mixing rates of spherical harmonic particles. Therefore, the influences of rotation speed and particle sphericity on the mixing rate of spherical harmonic particles are significant and cumulative, while the influences of the shape parameter on the particle mixing rate are of minor importance.

4.4. Dynamic angle of repose of particles

When the granular materials are completely mixed, the dynamic angle of repose for spheres and spherical harmonic granular materials with varying sphericity and shape parameters are counted, illustrated in Fig. 13. The angle of repose of different morphological particles

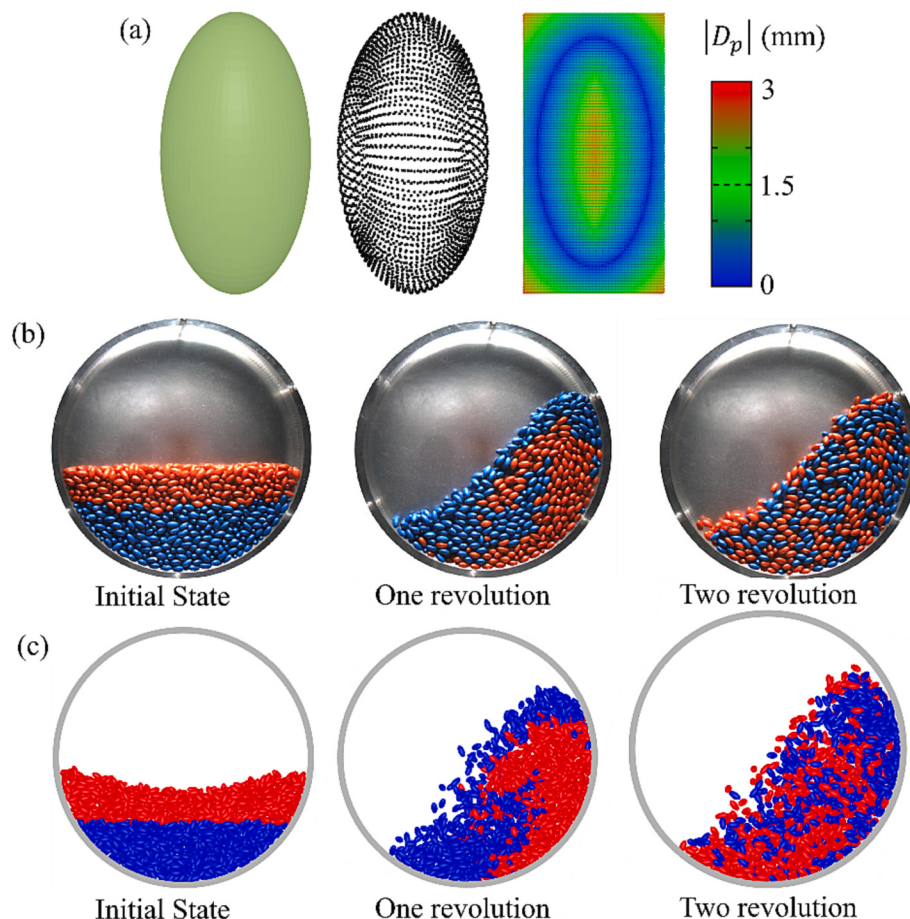


Fig. 7. Comparison of experimental [78] and simulation results of ellipsoidal mixing processes: (a) an ellipsoidal particle constructed from the spherical harmonic function and level set functions; (b) experimental results; (c) simulation results.

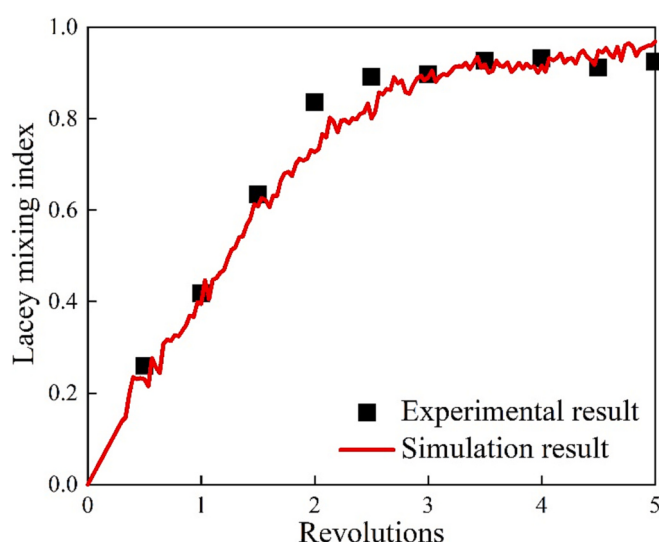


Fig. 8. Comparison of experimental [78] and simulation results for the time history of the Lacey Mixed Index.

increases with increasing rotational speeds. Spheres have a smaller angle of repose than spherical harmonic particles, and the particle sphericity has a negligible effect on the angle of repose of spherical harmonic particles. This is because shape deviations at the individual particle scale may be offset or compensated in the granular system at the

macroscopic scale [79]. When the shape parameter $N < 5$, the angle of repose of the spherical harmonic particles increases with increasing the shape parameter. When the parameter $N > 5$, the shape parameter has basically no effect on the angle of repose of particles. This is because the variation of particle shapes with shape parameter N becomes more pronounced when the parameter $N < 5$, illustrated in Fig. 5. Convex particles with smooth surfaces are gradually transformed into concave particles with uneven properties. Concave particles have a stronger interlocking than convex particles, which leads to a greater dynamic angle of repose for concave particles. When the parameter $N > 5$, the concavity of the particle surface becomes more pronounced, while the basic morphology does not change significantly. This indicates that the surface unevenness has insignificant effects on the dynamic angle of repose of particles.

4.5. Average coordination number between particles

The average coordination number can be used to reflect the contact pattern of particles on the micro-scale, which affects the motion and mixing properties of the granular material on the macro-scale [80]. Fig. 14 shows the average coordination number of spherical and spherical harmonic granular materials for various rotational speeds. The coordination number of differently shaped particles is larger at 0s than at 50s, and it decreases with increasing the rotational speed. This is because all particles fall under gravity and form a close contact mode at the initial moment. As the drum rotates, the particles slide and rotate with each other, which makes the granular system form a loose contact mode. As the rotational speed increases, the particles have a greater flowability, which results in a granular system with a looser contact

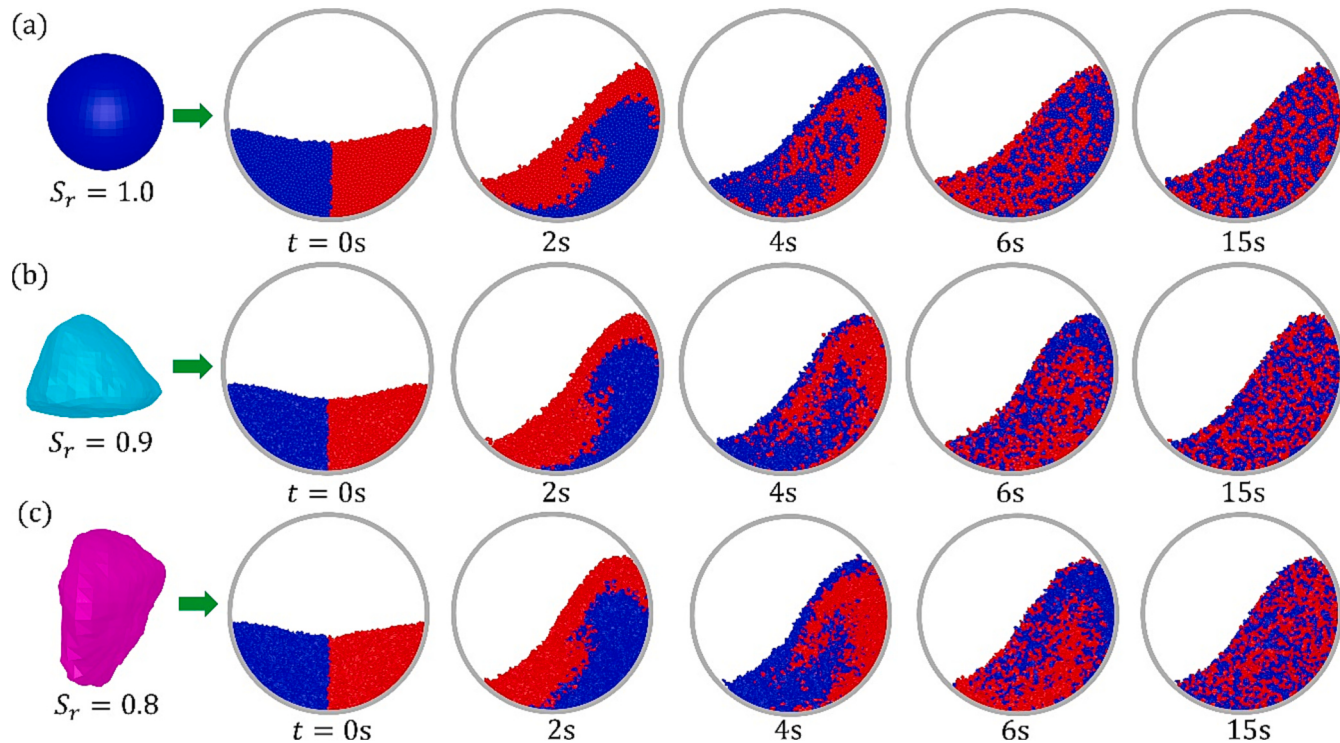


Fig. 9. Temporal evolutions of the mixing patterns of granular materials with various sphericity at 30 rpm: (a) $S_r = 1.0$; (b) $S_r = 0.9$; (c) $S_r = 0.8$.

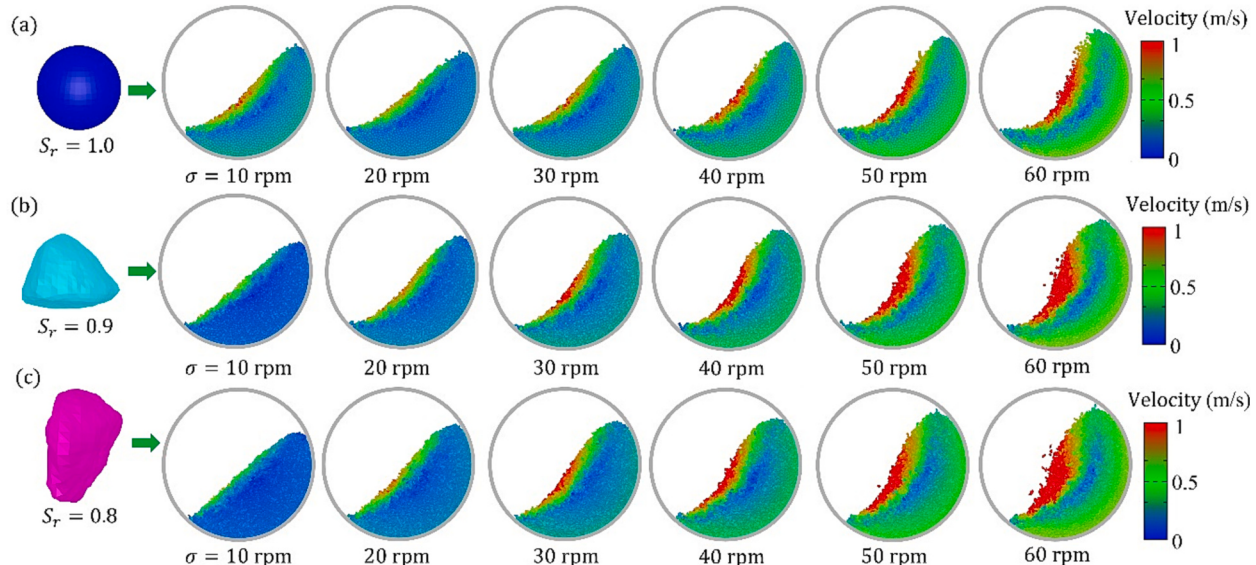


Fig. 10. Velocity distributions of granular materials with different sphericity within the rotating drum: (a) $S_r = 1.0$; (b) $S_r = 0.9$; (c) $S_r = 0.8$.

mode and a smaller average coordination number. In addition, spheres have a smaller average coordination number than spherical harmonic particles, and the coordination number of spherical harmonic particles tends to increase with decreasing particle sphericity. When the shape parameter $N < 5$, the coordination number of the spherical harmonic particles increases with increasing the shape parameter. When the parameter $N > 5$, the parameter N has basically little impact on the coordination number of the granular system. The contact modes of particles are changed by the particle shape on the micro-scale, and concave particles with more unevenness have closer contact modes.

4.6. Total energies of the granular system

The rotating drum acts as an essential mechanism for transferring external energy, effectively driving and facilitating the movement and mixing of the granular system [81]. Fig. 15 indicates the time histories of the translational and rotational kinetic energies of spherical and spherical harmonic granular materials at different rotational speeds. Upon the initiation of drum rotation, spherical harmonic granular systems exhibit greater energies required to transition from a static packing regime to a moving regime. This can be attributed to the closer contact mode and more stable packing structure inherent to spherical harmonic particles. After a rotating time surpassing 3s, the granular material has a

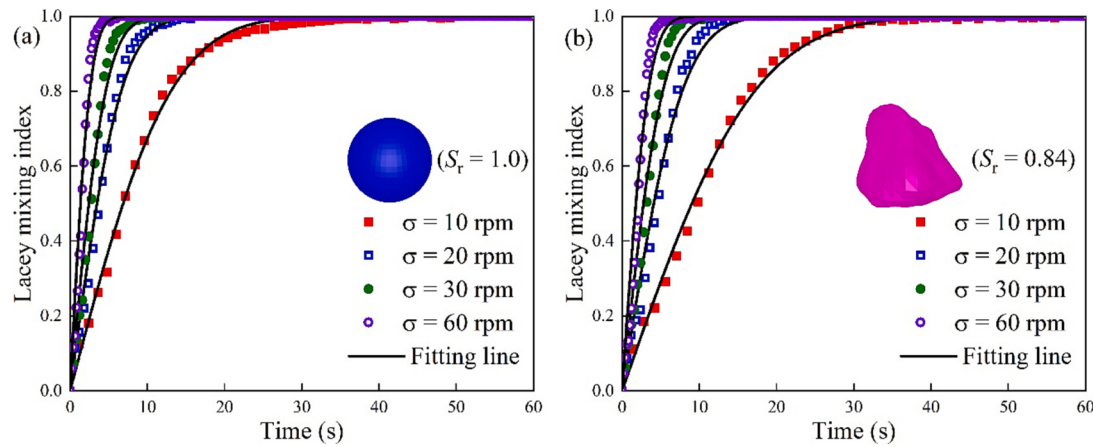


Fig. 11. Time evolutions of Lacey mixing index of spherical and spherical harmonic particles under various rotational speeds: (a) spherical granular materials; (b) spherical harmonic granular materials.

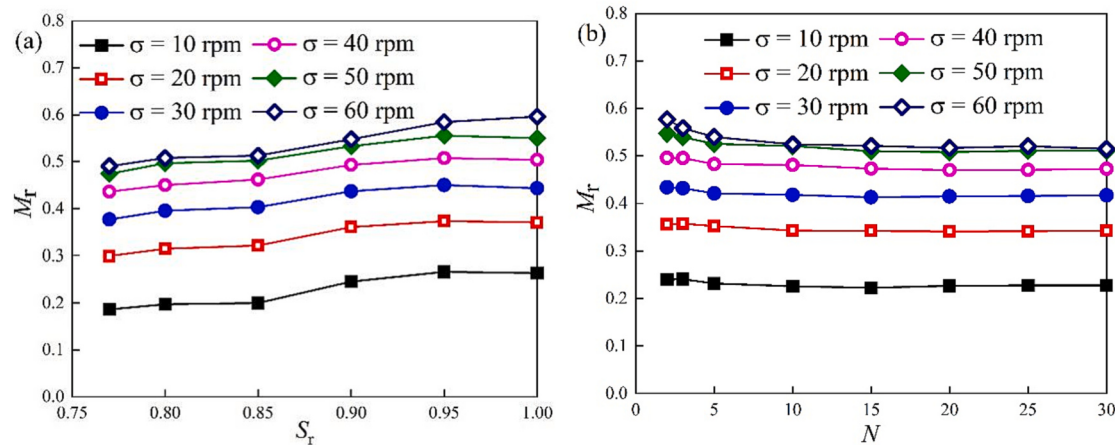


Fig. 12. Influences of particle sphericity (S_r) and shape parameter (N) on the mixing rate of granular materials: (a) particle sphericity S_r ; (b) shape parameter N .

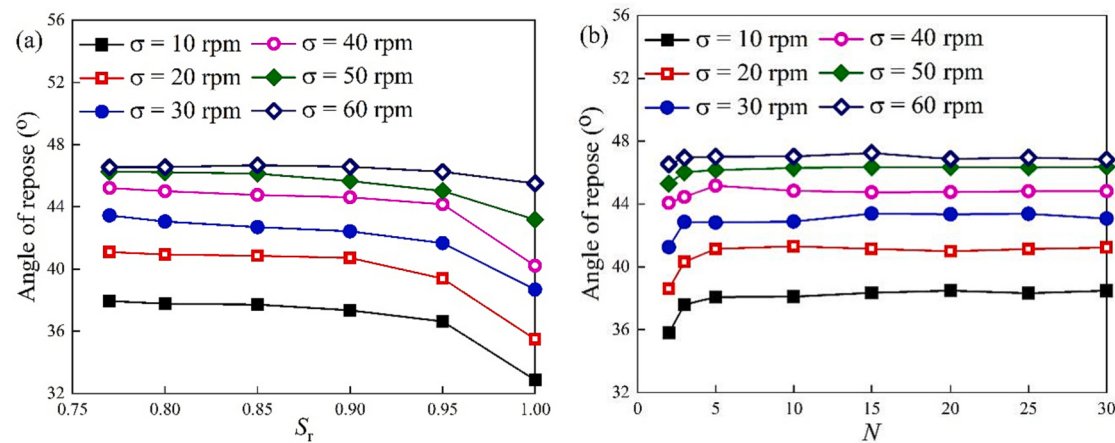


Fig. 13. Influences of particle sphericity (S_r) and shape parameter (N) on the dynamic angle of repose of granular materials: (a) particle sphericity S_r ; (b) shape parameter N .

stabilized kinetic energy. With an escalation in rotating speeds, the kinetic energies of the granular material escalate accordingly. Additionally, the particle shapes and rotating speeds yield a combined influence on the translational and rotational kinetic energies of the granular material. Hence, an analysis utilizing the average kinetic energy within the 3–14 s range effectively elucidates the impacts of particle sphericity and

shape parameters on the kinetic energy of granular systems.

Fig. 16 indicates the average translational and rotational kinetic energies of particles with various sphericity and shape parameters. As the particle sphericity increases, the translational kinetic energies of the spherical harmonic granular system decrease, and the rotational kinetic energies increase. This variation property of the system kinetic energy

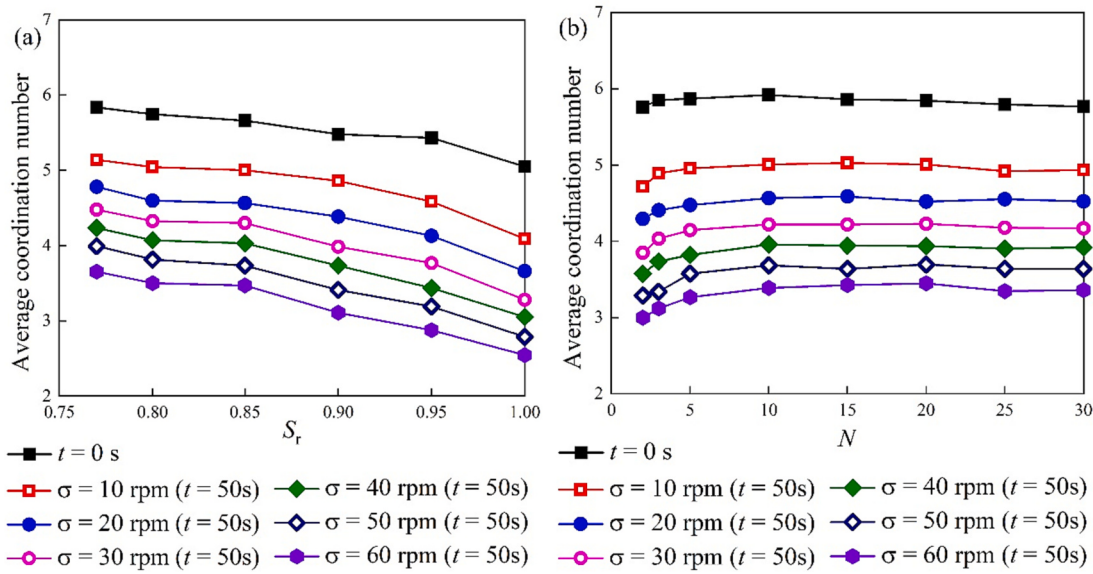


Fig. 14. Influences of particle sphericity (S_r) and shape parameter (N) on the average coordination number of granular materials: (a) particle sphericity S_r ; (b) shape parameter N .

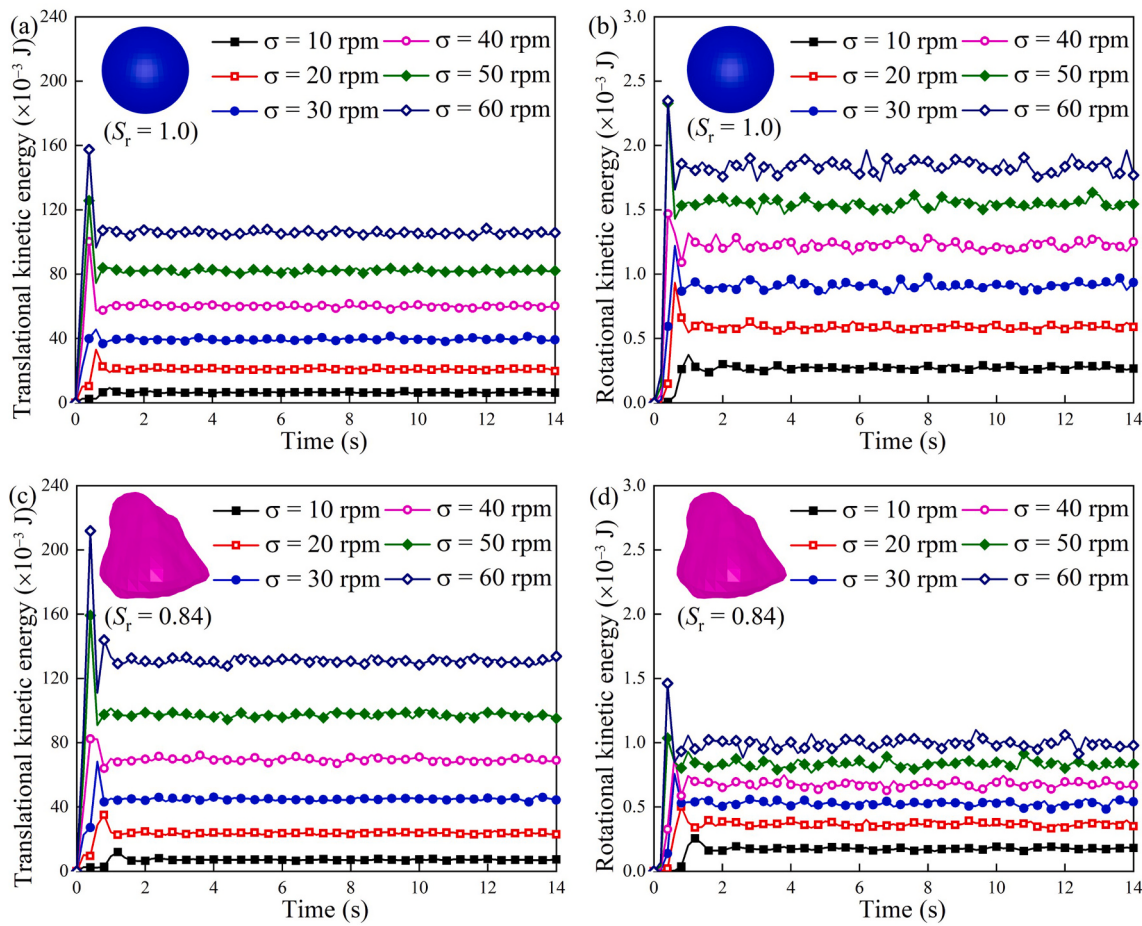


Fig. 15. Time variation of translational (a,c) and rotational kinetic energies (b,d) of spherical and spherical harmonic particles: (a-b) spherical particles; (c-d) spherical harmonic particles.

with particle sphericity becomes more significant as the rotational velocity increases. When the shape parameter $N < 5$, the translational kinetic energies of the spherical harmonic particles increase, and their

rotational kinetic energies decrease as the shape parameter increases. When the parameter $N > 5$, the shape parameter has basically no impact on the kinetic energies of particles. The spherical harmonic particle with

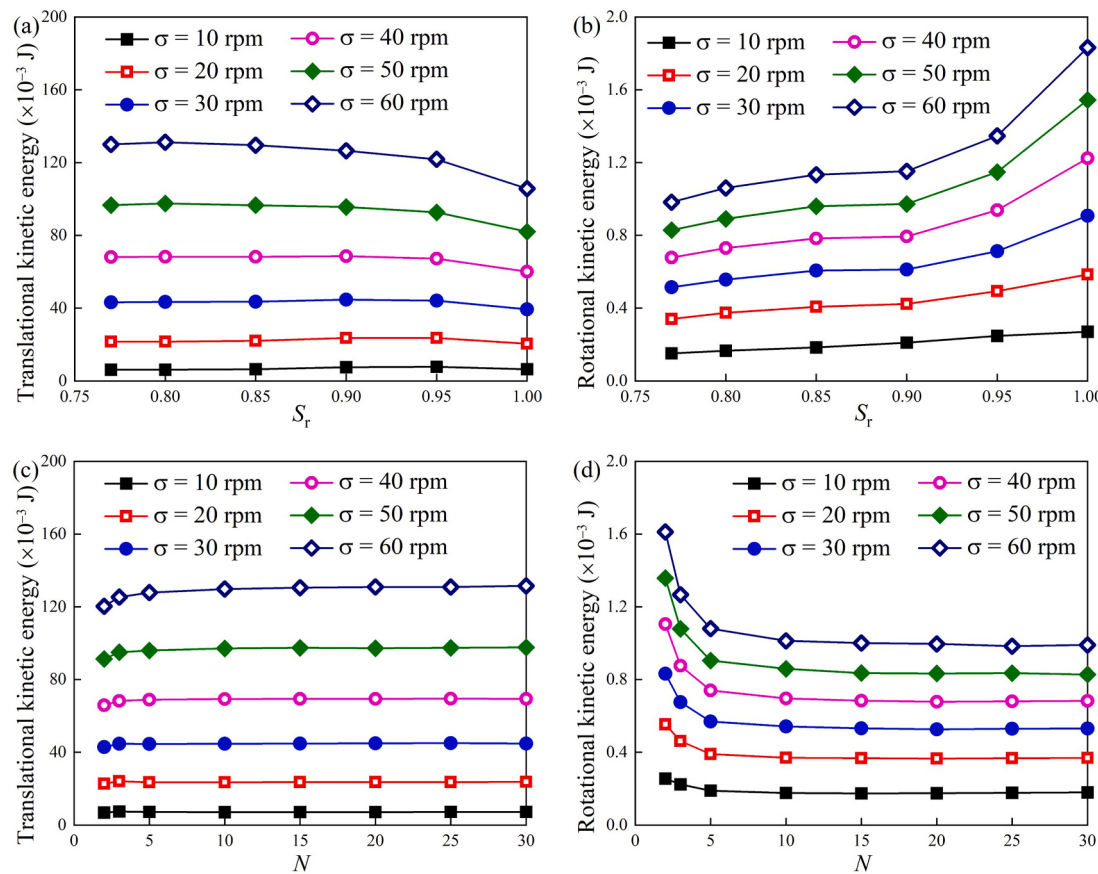


Fig. 16. Influences of particle sphericity S_r and shape parameter N on the translational (a,c) and rotational kinetic energies (b,d) of granular materials: (a-b) particle sphericity S_r ; (c-d) shape parameter N .

smaller sphericity and larger shape parameter has stronger interlocking, which limits relative rotation and rolling between particles. Although the smaller sphericity and larger shape parameter improve the conversion efficiencies of the outer energies into the spherical harmonic granular system, this decreases the mixing rate of the granular system.

4.7. Normal contact forces of particles

The contact forces between particles are available for characterizing the stabilization and the transfer of force chains within the granular material, which strongly relates to the underlying mechanisms of the mixing motion of the granular material [82]. Fig. 17(a-b) shows the probability density functions (PDF) of the normal contact forces of spherical and spherical harmonic granular materials at different rotational speeds. The probabilities of large normal contact forces of differently shaped particles increase with increasing the rotational speed. This is because more external energies are transferred to the granular system at greater rotating speeds, which makes the collisions between particles more violent. In addition, the influences of the particle sphericity and shape parameter on the probability density functions of the normal contact forces of granular materials are investigated, illustrated in Fig. 17(c-d). The probabilities of large contact forces of particles increase with decreasing the sphericity or increasing the shape parameter. Concave particles with more uneven surfaces have more collisions, strong interlocking and lower flowability, which results in lower mixing degrees of the granular system. Thus, the particle morphology induces variations in interparticle contact forces on the micro-scale. These contact forces are transmitted within the granular system through the force chain network, which may further cause a transition in the mixing behaviors of the granular system on the macro-

scale.

5. Conclusions

In this paper, spheres and concave-shaped particles are modeled by spherical harmonic functions, and the normal overlaps and directions between particles are determined through the utilization of the level-set method. Through extensive DEM simulations, this paper investigates the effects of particle sphericity, shape parameter and rotational speed on the mixing pattern, velocity distribution, Lacey mixing index, dynamic angle of repose, average coordination number, system kinetic energy and normal contact force. Results show that rotational speed and particle sphericity have a significant and superimposed effect on the mixing rate of spherical harmonic particles, whereas surface unevenness has little effect on the mixing rate of particles. Spheres have faster mixing rates than spherical harmonic particles, and the mixing rate of spherical harmonic particles decreases when the particle sphericity decreases or when the shape parameter increases. Spherical harmonic particles with smaller sphericity and larger shape parameters lead to larger average coordination numbers and closer contact modes, which constrain the rotation and rolling of particles. Concave particles have closer contact and greater collision forces than convex particles, which leads to higher coordination numbers, larger dynamic angles of repose, and stronger interlocking. Although the close contact pattern improves the conversion efficiencies of the external energies into the spherical harmonic granular system and increases the collision forces between particles, the stronger interlocking reduces the mixing rate of granular materials.

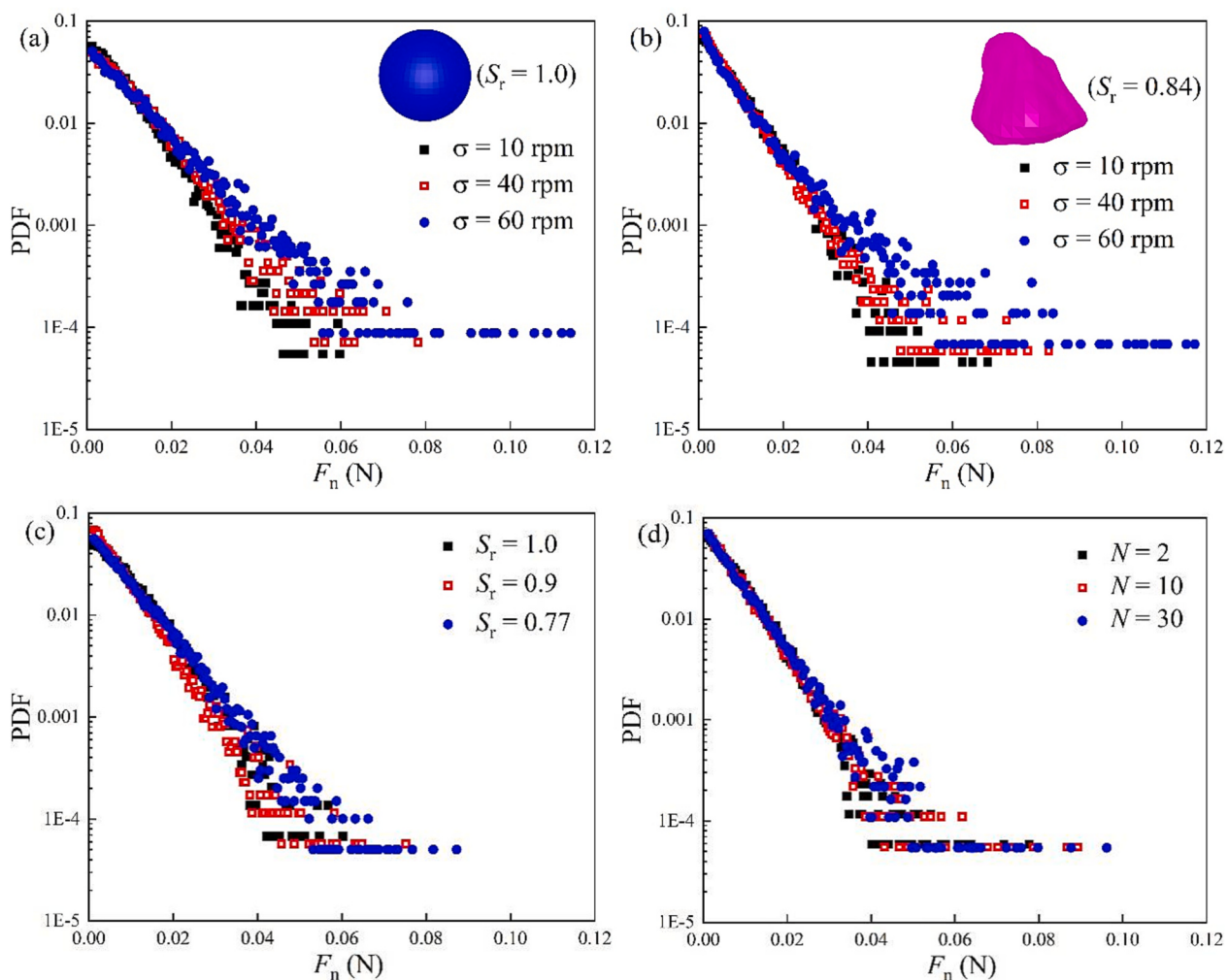


Fig. 17. Effects of the rotational speed (a-b), particle sphericity (c) and shape parameter (d) on the probability density functions of the normal contact forces for spherical and spherical harmonic granular materials.

Compliance with ethical standards

Conflicts of Interest: The authors declare that there is no conflict of interest regarding the publication of this paper.

CRediT authorship contribution statement

Siqiang Wang: Data curation, Writing – original draft, Formal analysis. **Dongfang Liang:** Methodology, Validation. **Shunying Ji:** Conceptualization, Writing – review & editing, Supervision, Funding acquisition.

Declaration of Competing Interest

The authors declare that they have no known competing financial interests or personal relationships that could have appeared to influence the work reported in this paper.

Data availability

Data will be made available on request.

Acknowledgments

The A_{nm} coefficients are derived from Dr. Garboczi's real particle

morphology database, available at <ftp://nist.gov/pub/bfrl/garboczi/Particle-shape-database/MA111-7/>. We appreciate this valuable public service.

This study is financially supported by the National Key Research and Development Program of China (Grant No. 2021YFA1500302), the National Natural Science Foundation of China (Grant Nos. 42176241, 52192693, U20A20327, and 12202095), the Dalian Scientific Innovation Foundation of China (Grant No. 2022RQ004), and the China Postdoctoral Science Foundation (Grant No. 2022M710587).

References

- [1] R.G. Sherritt, J. Chaouki, A.K. Mehrotra, L.A. Behie, Axial dispersion in the three-dimensional mixing of particles in a rotating drum reactor, *Chem. Eng. Sci.* 58 (2003) 401–415.
- [2] G.G. Pereira, S. Pucilowski, K. Lifman, P.W. Cleary, Streak patterns in binary granular media in a rotating drum, *Appl. Math. Model.* 35 (2011) 1638–1646.
- [3] S. Yang, Y. Sun, L. Zhang, J.W. Chew, Numerical study on the axial segregation dynamics of a binary-size granular mixture in a three-dimensional rotating drum, *Phys. Fluids* 29 (2017), 103302.
- [4] P.A. Cundall, O.D.L. Strack, A discrete numerical model for granular assemblies, *Géotechnique* 29 (1979) 47–65.
- [5] Z. Cui, Y. Zhao, Y. Chen, X. Liu, Z. Hua, C. Zhou, J. Zheng, Transition of axial segregation patterns in a long rotating drum, *Particuology* 13 (2014) 128–133.
- [6] S. Yang, L. Zhang, K. Luo, J.W. Chew, DEM investigation of the axial dispersion behavior of a binary mixture in the rotating drum, *Powder Technol.* 330 (2018) 93–104.
- [7] S. Wang, M. Zhuravkov, S. Ji, Granular flow of cylinder-like particles in a cylindrical hopper under external pressure based on DEM simulations, *Soft Matter* 16 (2020) 7760–7777.

- [8] M.M.H.D. Arntz, H.H. Beeltink, W.K. den Otter, W.J. Briels, R.M. Boom, Segregation of granular particles by mass, radius, and density in a horizontal rotating drum, *AICHE J.* 60 (2014) 50–59.
- [9] B. Alchikh-Sulaiman, M. Alian, F. Ein-Mozaffari, A. Lohi, S.R. Upreti, Using the discrete element method to assess the mixing of polydisperse solid particles in a rotary drum, *Particuology* 25 (2016) 133–142.
- [10] A. Mesnier, M. Rouabah, C. Cogné, R. Pczalski, S. Vessot-Craestes, P. Vacus, J. Andrieu, Contact heating of bi-dispersed milli-beads in a rotary drum. Mechanical segregation impact on temperature distribution and on heating kinetic analyzed by DEM simulation, *Powder Technol.* 354 (2019) 240–246.
- [11] M. Jiang, Y. Zhao, G. Liu, J. Zheng, Enhancing mixing of particles by baffles in a rotating drum mixer, *Particuology* 9 (2011) 270–278.
- [12] F. Yu, G. Zhou, J. Xu, W. Ge, Enhanced axial mixing of rotating drums with alternately arranged baffles, *Powder Technol.* 286 (2015) 276–287.
- [13] M. Halidan, G.R. Chandratileke, K.J. Dong, A.B. Yu, Mixing performance of ribbon mixers: effects of operational parameters, *Powder Technol.* 325 (2018) 92–106.
- [14] H. Chen, Y.G. Xiao, Y.L. Liu, Y.S. Shi, Effect of Young's modulus on DEM results regarding transverse mixing of particles within a rotating drum, *Powder Technol.* 318 (2017) 507–517.
- [15] S. Yang, H. Wang, Y. Wei, J. Hu, J.W. Chew, Flow dynamics of binary mixtures of nonspherical particles in the rolling-regime rotating drum, *Powder Technol.* 361 (2020) 930–942.
- [16] S. Wang, Y. Fan, S. Ji, Interaction between super-quadratic particles and triangular elements and its application to hopper discharge, *Powder Technol.* 339 (2018) 534–549.
- [17] S.Y. He, J.Q. Gan, D. Pinson, A.B. Yu, Z.Y. Zhou, Flow regimes of cohesionless ellipsoidal particles in a rotating drum, *Powder Technol.* 354 (2019) 174–187.
- [18] S. He, J. Gán, D. Pinson, A. Yu, Z. Zhou, A discrete element method study of monodisperse mixing of ellipsoidal particles in a rotating drum, *Ind. Eng. Chem. Res.* 59 (2020) 12458–12470.
- [19] H. Ma, Y. Zhao, Investigating the flow of rod-like particles in a horizontal rotating drum using DEM simulation, *Granul. Matter* 20 (2018) 41.
- [20] S. Wang, S. Ji, Poly-superquadratic model for DEM simulations of asymmetrically shaped particles, *Comp. Part. Mech.* 9 (2022) 299–313.
- [21] N. Gui, X. Yang, J. Tu, S. Jiang, Numerical simulation and analysis of mixing of polygonal particles in 2D rotating drums by SIPHPM method, *Powder Technol.* 318 (2017) 248–262.
- [22] N. Gui, X. Yang, J. Tu, S. Jiang, Z. Zhang, Numerical simulation of tetrahedral particle mixing and motion in rotating drums, *Particuology* 39 (2018) 1–11.
- [23] F. Yu, S. Zhang, G. Zhou, Y. Zhang, W. Ge, Geometrically exact discrete-element-method (DEM) simulation on the flow and mixing of spherocylinders in horizontal drums, *Powder Technol.* 336 (2018) 415–425.
- [24] D. Höhner, S. Wirtz, V. Scherer, Experimental and numerical investigation on the influence of particle shape and shape approximation on hopper discharge using the discrete element method, *Powder Technol.* 235 (2013) 614–627.
- [25] D. Höhner, S. Wirtz, V. Scherer, A study on the influence of particle shape and shape approximation on particle mechanics in a rotating drum using the discrete element method, *Powder Technol.* 253 (2014) 256–265.
- [26] L. Liu, S. Ji, A new contact detection method for arbitrary dilated polyhedra with potential function in discrete element method, *Int. J. Numer. Methods Eng.* 121 (2020) 5742–5765.
- [27] W. Zhong, A. Yu, X. Liu, Z. Tong, H. Zhang, DEM/CFD-DEM modelling of non-spherical particulate systems: theoretical developments and applications, *Powder Technol.* 302 (2016) 108–152.
- [28] Y.T. Feng, Thirty years of developments in contact modelling of nonspherical particles in DEM: a selective review, *Acta Mech. Sinica* 39 (2023), 722343.
- [29] A.D. Rakotonirina, J.-Y. Delenne, F. Radjai, A. Wachs, Grains3D, a flexible DEM approach for particles of arbitrary convex shape—part III: extension to non-convex particles modelled as glued convex particles, *Comp. Part. Mech.* 6 (2019) 55–84.
- [30] C.Q. Li, W.J. Xu, Q.S. Meng, Multi-sphere approximation of real particles for DEM simulation based on a modified greedy heuristic algorithm, *Powder Technol.* 286 (2015) 478–487.
- [31] N. Govender, D.N. Wilke, C.-Y. Wu, J. Khinast, P. Pizette, W. Xu, Hopper flow of irregularly shaped particles (non-convex polyhedra): GPU-based DEM simulation and experimental validation, *Chem. Eng. Sci.* 188 (2018) 34–51.
- [32] Z. Liu, Y. Zhao, Multi-super-ellipsoid model for nonspherical particles in DEM simulation, *Powder Technol.* 361 (2020) 190–202.
- [33] S. Wang, S. Ji, Flow characteristics of nonspherical granular materials simulated with multi-superquadratic elements, *Particuology* 54 (2021) 25–36.
- [34] L. Meng, C. Wang, X. Yao, Non-convex shape effects on the dense random packing properties of assembled rods, *Phys. A: Stat. Mech. Appl.* 490 (2018) 212–221.
- [35] H. Kruggel-Emden, S. Rickelt, S. Wirtz, V. Scherer, A study on the validity of the multi-sphere discrete element method, *Powder Technol.* 188 (2008) 153–165.
- [36] C. Li, Y. Peng, P. Zhang, C. Zhao, The contact detection for heart-shaped particles, *Powder Technol.* 346 (2019) 85–96.
- [37] B. Zhou, J. Wang, Generation of a realistic 3D sand assembly using X-ray micro-computed tomography and spherical harmonic-based principal component analysis, *Int. J. Numer. Anal. Methods Geomech.* 41 (2017) 93–109.
- [38] S. Liu, F. Chen, W. Ge, P. Ricoux, NURBS-based DEM for nonspherical particles, *Particuology* 49 (2020) 65–76.
- [39] M.V. Craveiro, A. Gay Neto, P. Wriggers, Contact between rigid convex NURBS particles based on computer graphics concepts, *Comput. Methods Appl. Mech. Eng.* 386 (2021), 114097.
- [40] G. Mollon, J. Zhao, 3D generation of realistic granular samples based on random fields theory and Fourier shape descriptors, *Comput. Methods Appl. Mech. Eng.* 279 (2014) 46–65.
- [41] Z. Lai, Q. Chen, L. Huang, Fourier series-based discrete element method for computational mechanics of irregular-shaped particles, *Comput. Methods Appl. Mech. Eng.* 362 (2020), 112873.
- [42] J.M. Harmon, K. Karapiperis, L. Li, S. Moreland, J.E. Andrade, Modeling connected granular media: particle bonding within the level set discrete element method, *Comput. Methods Appl. Mech. Eng.* 373 (2021), 113486.
- [43] Z. Lai, S. Zhao, J. Zhao, L. Huang, Signed distance field framework for unified DEM modeling of granular media with arbitrary particle shapes, *Comput. Mech.* 70 (2022) 763–783.
- [44] Y.T. Feng, An energy-conserving contact theory for discrete element modelling of arbitrarily shaped particles: basic framework and general contact model, *Comput. Methods Appl. Mech. Eng.* 373 (2021), 113454.
- [45] Y.T. Feng, An energy-conserving contact theory for discrete element modelling of arbitrarily shaped particles: contact volume based model and computational issues, *Comput. Methods Appl. Mech. Eng.* 373 (2021), 113493.
- [46] E.J. Garboczi, J.W. Bullard, 3D analytical mathematical models of random star-shape particles via a combination of X-ray computed microtomography and spherical harmonic analysis, *Adv. Powder Technol.* 28 (2017) 325–339.
- [47] T. Ueda, Estimation of three-dimensional particle size and shape characteristics using a modified 2D–3D conversion method employing spherical harmonic-based principal component analysis, *Powder Technol.* 404 (2022), 117461.
- [48] R. Capozza, K.J. Hanley, A hierarchical, spherical harmonic-based approach to simulate abradable, irregularly shaped particles in DEM, *Powder Technol.* 378 (2021) 528–537.
- [49] W. Xu, B. Zhang, M. Jia, W. Wang, Z. Gong, J. Jiang, Discrete element modeling of 3D irregular concave particles: transport properties of particle-reinforced composites considering particles and soft interphase effects, *Comput. Methods Appl. Mech. Eng.* 394 (2022), 114932.
- [50] W. Xu, M. Jia, W. Guo, W. Wang, B. Zhang, Z. Liu, J. Jiang, GPU-based discrete element model of realistic non-convex aggregates: mesoscopic insights into ITZ volume fraction and diffusivity of concrete, *Cem. Concr. Res.* 164 (2023), 107048.
- [51] W. Xu, W. Wang, W. Guo, M. Jia, Y. Jiao, Soft interphase volume fraction of composites containing arbitrarily shaped mono- / poly-disperse fillers: theoretical and numerical investigations, *Powder Technol.* 424 (2023), 118556.
- [52] J.Y. Nie, D.Q. Li, Z.J. Cao, B. Zhou, A.J. Zhang, Probabilistic characterization and simulation of realistic particle shape based on sphere harmonic representation and Nataf transformation, *Powder Technol.* 360 (2020) 209–220.
- [53] S. Wang, Z. Wei, S. Ji, Investigation of the flow characteristics of spherical harmonic particles using the level set method, *Powder Technol.* 413 (2023), 118069.
- [54] W. Xiong, J. Wang, Gene mutation of particle morphology through spherical harmonic-based principal component analysis, *Powder Technol.* 386 (2021) 176–192.
- [55] X. Wang, Z.Y. Yin, H. Xiong, D. Su, Y. Feng, A spherical-harmonic-based approach to discrete element modeling of 3D irregular particles, *Int. J. Numer. Methods Eng.* 122 (2021) 5626–5655.
- [56] Y.T. Feng, An effective energy-conserving contact modelling strategy for spherical harmonic particles represented by surface triangular meshes with automatic simplification, *Comput. Methods Appl. Mech. Eng.* 379 (2021), 113750.
- [57] E.J. Garboczi, Three-dimensional mathematical analysis of particle shape using X-ray tomography and spherical harmonics: application to aggregates used in concrete, *Cem. Concr. Res.* 32 (2002) 1621–1638.
- [58] U. Radvilaitė, Á. Ramírez-Gómez, R. Kacianauskas, Determining the shape of agricultural materials using spherical harmonics, *Comput. Electron. Agric.* 128 (2016) 160–171.
- [59] I. Vlahinić, R. Kawamoto, E. Andò, G. Viggiani, J.E. Andrade, From computed tomography to mechanics of granular materials via level set bridge, *Acta Geotech.* 12 (2017) 85–95.
- [60] R. Kawamoto, E. Andò, G. Viggiani, J.E. Andrade, All you need is shape: predicting shear banding in sand with LS-DEM, *J. Mech. Phys. Solids* 111 (2018) 375–392.
- [61] S. Wang, S. Ji, A unified level set method for simulating mixed granular flows involving multiple nonspherical DEM models in complex structures, *Comput. Methods Appl. Mech. Eng.* 393 (2022), 114802.
- [62] J.M. Harmon, D. Arthur, J.E. Andrade, Level set splitting in DEM for modeling breakage mechanics, *Comput. Methods Appl. Mech. Eng.* 365 (2020), 112961.
- [63] K.A. Buist, L.J.H. Seelen, N.G. Deen, J.T. Padding, J.A.M. Kuipers, On an efficient hybrid soft and hard sphere collision integration scheme for DEM, *Chem. Eng. Sci.* 153 (2016) 363–373.
- [64] B.P.B. Hoomans, J.A.M. Kuipers, W.J. Briels, W.P.M. van Swaaij, Discrete particle simulation of bubble and slug formation in a two-dimensional gas-fluidised bed: a hard-sphere approach, *Chem. Eng. Sci.* 51 (1996) 99–118.
- [65] A.B. Morris, S. Pannala, Z. Ma, C.M. Hrenya, Development of soft-sphere contact models for thermal heat conduction in granular flows, *AICHE J.* 62 (2016) 4526–4535.
- [66] R. Kawamoto, E. Andò, G. Viggiani, J.E. Andrade, Level set discrete element method for three-dimensional computations with triaxial case study, *J. Mech. Phys. Solids* 91 (2016) 1–13.
- [67] Z.Y. Zhou, R.P. Zou, D. Pinson, A.-B. Yu, Dynamic simulation of the packing of ellipsoidal particles, *Ind. Eng. Chem. Res.* 50 (2011) 9787–9798.
- [68] S. Wang, Z. Zhou, S. Ji, Radial segregation of a gaussian-dispersed mixture of superquadratic particles in a horizontal rotating drum, *Powder Technol.* 394 (2021) 813–824.
- [69] X. Liu, J. Gan, W. Zhong, A. Yu, Particle shape effects on dynamic behaviors in a spouted bed: CFD-DEM study, *Powder Technol.* 361 (2020) 349–362.

- [70] F. Yu, Y. Zhang, Y. Zheng, M. Han, G. Chen, Z. Yao, Comparison of different effective diameter calculating methods for spherocylinders by geometrically exact DEM simulations, *Powder Technol.* 360 (2020) 1092–1101.
- [71] K. Dong, C. Wang, A. Yu, A novel method based on orientation discretization for discrete element modeling of nonspherical particles, *Chem. Eng. Sci.* 126 (2015) 500–516.
- [72] H. Wadell, Sphericity and roundness of rock particles, *J. Geol.* 41 (1933) 310–331.
- [73] J.W. Bullard, E.J. Garboczi, Defining shape measures for 3D star-shaped particles: Sphericity, roundness, and dimensions, *Powder Technol.* 249 (2013) 241–252.
- [74] B. Zhou, J. Wang, H. Wang, Three-dimensional sphericity, roundness and fractal dimension of sand particles, *Géotechnique* 68 (2018) 18–30.
- [75] Y. Zhao, J.W. Chew, Discrete element method study on hopper discharge behaviors of binary mixtures of nonspherical particles, *AICHE J.* 66 (2020), e16254.
- [76] P.M.C. Lacey, Developments in the theory of particle mixing, *J. Appl. Chem.* 4 (1954) 257–268.
- [77] S. He, J. Gan, D. Pinson, Z. Zhou, Transverse mixing of ellipsoidal particles in a rotating drum, *EPJ Web Conf.* 140 (2017) 06018.
- [78] Y. You, Y. Zhao, Discrete element modelling of ellipsoidal particles using super-ellipsoids and multi-spheres: a comparative study, *Powder Technol.* 331 (2018) 179–191.
- [79] S. Ji, H.H. Shen, Effect of contact force models on granular flow dynamics, *J. Eng. Mech.-Asce.* 132 (2006) 1252–1259.
- [80] Y. Guo, C. Wassgren, W. Ketterhagen, B. Hancock, J. Curtis, Discrete element simulation studies of angles of repose and shear flow of wet, flexible fibers, *Soft Matter* 14 (2018) 2923–2937.
- [81] S. Ji, S. Wang, Z. Zhou, Influence of particle shape on mixing rate in rotating drums based on super-quadratic DEM simulations, *Adv. Powder Technol.* 31 (2020) 3540–3550.
- [82] A.L. Thomas, Z. Tang, K.E. Daniels, N.M. Vriend, Force fluctuations at the transition from quasi-static to inertial granular flow, *Soft Matter* 15 (2019) 8532–8542.